An Analysis of Muscle Co-contraction Strategies Using Dynamic Optimization and Electromyography While Walking on Uneven Surfaces

Banin M. Al-Shimari[1,*], Vivian T. Nguyen[1], Marco J. Perizzolo[2], Sarah L. Manske[1,3,4], Ranita H. K. Manocha[1,3,5], W. Brent Edwards[1,3,6], Michael J. Asmussen[3,6,7]

[1]Department of Biomedical Engineering, University of Calgary, Calgary T2N 1N4, Canada

[2]Department of Biology, Mount Royal University, Calgary T3E 6K6, Canada

[3]McCaig Institute for Bone and Joint Health, University of Calgary, Calgary T2N 4Z6, Canada

[4]Department of Radiology, Cumming School of Medicine, University of Calgary, Calgary T2N 2T9, Canada

[5]Division of Physical Medicine and Rehabilitation, Cumming School of Medicine, University of Calgary, Calgary T2N 1N4, Canada

[6]Human Performance Laboratory, Faculty of Kinesiology, University of Calgary, Calgary T2N 1N4, Canada

[7]Department of Kinesiology, Vancouver Island University, Nanaimo V9R 5S5, British Columbia

*banin.alshimari1@ucalgary.ca

ABSTRACT

Walking requires coordinated muscle activation, including co-contraction of opposing muscle groups, to maintain joint stability. The purpose of this study was to compare conventional measures of co-contraction with a novel muscle moment co-contraction index. Eighteen participants walked at 0.8 m/s and 1.6 m/s in three uneven footwear conditions: 1) 1 cm medial-posterior ridge (MPR), 2) 1 cm lateral-posterior ridge (LPR), 3) a no-ridge condition (NR). We estimated muscle forces using electromyography (EMG) constrained dynamic optimization. Co-contraction of the peroneus longus with the tibialis anterior as well as the soleus and gastrocnemius medialis was calculated during early and mid-stance using two co-contraction methods: (1) an EMG-Based co-contraction index, using normalized EMG only, and (2) an EMG-Track method, a novel muscle-moment-based index derived from dynamically optimized muscle forces. Overall, the mean co-contraction index predicted by the EMG-Track method was significantly lower than that predicted by the EMG-Based method. Significant interaction effects were observed using EMG-Track, but not EMG-Based (e.g., PL/MG early stance: $F_{(2,34)}$=6.779, p=0.003, η_g^2=0.020). Our findings support a muscle moment-based approach to interpreting co-contraction, with implications for populations for whom co-contraction reflects stability during locomotion and/or overall locomotor function.

INTRODUCTION

Walking may seem simple, as it appears to be effortless. Taking a single step, however, requires complex coordination of over one hundred structures, including muscles, tendons, and ligaments, in the foot-ankle joint complex to move the body forward while maintaining balance[1]. Walking is further complicated by the requirement to maintain stability in the mediolateral direction, a direction in which humans are inherently less stable[1]. Thus, humans use several strategies to remain upright while walking. One of the most important strategies to maintain balance while walking is the "foot placement strategy", whereby when a person experiences a sudden imbalance in the medial or lateral direction, they can adjust their foot spatially and place it more medially or laterally to maintain stability[2]. However, this strategy is less effective on uneven surfaces, such as rocky trails, where maintaining stability is even more challenging. During this scenario, a corrective step may not be possible, and a person must make a correction during ground contact[3-5]. Humans and other terrestrial vertebrates have historically encountered uneven and ungroomed surfaces during locomotion. Humans incorporate different strategies to stay upright in these environments. Still, the specific strategies for mediolateral stability on uneven surfaces remain unclear when a foot placement strategy may not be feasible and stability must be maintained using different strategies.

When traversing an unstable environment, adaptations can also be made during the stance phase, when the foot is in contact with the ground. During stance, the neuromuscular system can modify its activity to remain upright. Muscular co-contraction, typically defined as the simultaneous activation or contraction of agonist and antagonist muscles at the joint level, may be necessary for maintaining stability while walking on uneven surfaces[6]. For instance, walking on unpredictable, unstable footwear increases co-contraction of the dorsiflexors and plantarflexors in the early and late stance phases of the gait cycle[7]. Similarly, adults who usually utilize ankle muscle co-contraction of the dorsiflexors and plantarflexors experience fewer and less severe falls on slippery surfaces[8]. Co-contraction in these unstable environments may be necessary to ensure joint stability and potentially whole-body stability during walking[7-9]. However, studies examining co-contraction often neglect other important intrinsic foot joints that may play a key role in stabilizing the body[7-10]. The subtalar joint is one of these joints essential for controlling the foot's motion in multiple planes, although primarily in the frontal plane (i.e., the mediolateral direction)[11].

Quantifying muscle co-contraction is important for evaluating neuromuscular control and understanding how opposing muscle groups contribute to joint stability during movement. However, the lack of a standardized method for calculating co-contraction has led to various computational approaches, each with its own limitations. One of the most common methods uses normalized electromyography (EMG) measurements because of their ease of use and applicability in clinical settings[12-14]. Although EMG is often used as a surrogate for muscle force, the relationship between EMG and muscle force is not always linear, particularly during dynamic activities such as walking[15]. Moreover, muscle force is influenced by intrinsic muscle factors, such as force-length-velocity relationships, and mechanical properties such as changes in moment arm as a function of joint angle/bone position and orientation, which EMG alone cannot capture[16-20]. Co-contraction measures, historically, have primarily been concerned with the interaction between agonist and antagonist muscles that stabilize or move a joint. In the absence of invasive measurements of direct muscle force, it is likely that the ideal method for calculating co-contraction involves using an estimate of muscle force, as it is muscle force, not simply a measure of muscle activation, that controls joint motion. Muscle moment-based co-contraction analysis, incorporating muscle force estimates and moment arms, provides an indirect, potentially more accurate measure of the muscular contributions to joint stability versus using muscle activations alone. Muscle force estimates are particularly relevant when assessing the mechanical outcomes of co-contraction, such as joint quasi-stiffness or load distribution. Despite the limitations of using EMG alone for co-contraction analyses, these co-contraction indices remain widely used in research and clinical settings[21-25].

Researchers often estimate muscle forces using optimization algorithms that minimize activations or forces to simulate efficient movement[26-28]. However, these methods may overlook agonist muscle synergies, individual recruitment strategies, and co-contraction patterns[26-28]. EMG-driven models address this potential issue by constraining predicted excitations with experimental EMG data, though they face limitations in accessing deep muscles and applying electrodes to all relevant muscles[27,29-31]. To address these challenges, researchers often exclude muscles, treat them as passive force generators, or use EMG data from a single muscle to represent a group of muscles with similar functional roles based on shared or common innervation [27,29-31]. In response to these limitations, hybrid approaches have been developed, coined "EMG-assisted" or "EMG-constrained" optimization[27,29-31]. These methods combine optimization techniques with EMG data to 1) estimate muscle excitations for muscles lacking EMG data, 2) minimally adjust muscle excitations to smooth out artifacts from EMG processing, and 3) include participant-specific muscle recruitment strategies.

EMG-constrained optimization has been used to quantify co-contraction across various tasks, including shoulder muscles during overhead handling[32], abdominal muscles during waste collection[31], and finger muscles during free motion and arm tasks[33],[34]. In the lower body, it has been applied to the hip in people with hip osteoarthritis during walking[29] and half-squat tasks.[35] While co-contraction has been examined in the cervical and trunk muscles[36,37], it has not been calculated using subtalar joint muscle moments during mediolateral perturbations when walking. Moreover, most prior methods rely on static optimization[26,38,39,] which overlooks time-dependent activation and contraction dynamics of muscles[38]. Therefore, the purpose of this study was to compare muscle co-contraction strategies when walking on mediolaterally uneven surfaces using 1) the conventional method typically used in the literature using EMG only, defined as "EMG-Based", and 2) an EMG-constrained dynamic optimization method, defined as "EMG-Track". To compare these methods, 18 healthy participants (9 females and 9 males; Body Mass: 80.17kg ± 12.69; Age: 22.78 ± 1.73) walked on a force-instrumented split-belt treadmill at 0.8 m/s and 1.6 m/s under three footwear conditions: a 1 cm medial-posterior ridge (MPR), which limited pronation; a 1 cm lateral-posterior ridge (LPR), which increased pronation; and a no-ridge (NR) condition.. Because the EMG-Track method reflects the mechanical and intrinsic properties of muscle, our first hypothesis was that it would be more sensitive to differences in co-contraction across footwear conditions and walking speeds than the EMG-Based method. Our secondary hypothesis was that co-contraction magnitude would differ, with the EMG-Track method expected to yield a lower co-contraction magnitude than the EMG-Based method.

RESULTS

In this study, we compared co-contraction obtained using the EMG-Based and EMG-Track methods across three muscle pairs: peroneus longus/tibialis anterior (PL/TA), peroneus longus/medial gastrocnemius (PL/MG), and peroneus longus/soleus (PL/SOL). This analysis was conducted across three footwear conditions (lateral posterior ridge (LPR), medial posterior ridge (MPR), and no ridge (NR)), two speeds (0.8 m/s and 1.6 m/s), and two methods of calculating co-contraction (EMG-Based and EMG-Track). We performed a 3-way repeated-measures ANOVA for early and mid-stance separately to determine differences in the two co-contraction methods in detecting changes in the co-contraction index across these factors. Co-contraction is likely important during early and mid-stance, and so analyses were limited to these periods.

Across all muscle pairs, the EMG-Track and EMG-Based methods produced distinct time-varying co-contraction profiles that differed in both magnitude and shape across early, mid-, and late stance (Figures 1–3). Descriptively, in all figures, early stance EMG-Track consistently showed a sharp initial drop in co-contraction index followed by a small condition-dependent peak. In contrast, EMG-Based curves were consistently higher and less sensitive to footwear changes. Overall, EMG-Track exhibited greater sensitivity to stance-phase dynamics and footwear-induced mediolateral instability, whereas EMG-Based curves remained more uniform in shape and amplitude.

Peroneus Longus/Tibialis Anterior (PL/TA) Muscle Pair

For the PL/TA muscle pair, EMG-Track co-contraction was descriptively elevated during early stance, with a pronounced peak immediately after initial contact. In contrast, EMG-based co-contraction showed a lower, more gradual profile during this period (Figure 1). As stance progressed into mid-stance, EMG-Track co-contraction declined markedly to its lowest values, while EMG-Based co-contraction remained comparatively higher and showed less temporal fluctuation. This resulted in a clear divergence between methods during mid-stance, with EMG-Track consistently showing values below EMG-Based across the central portion of the stance phase. In late stance, EMG-Track co-contraction increased rapidly, demonstrating a steep rise toward the end of stance, while EMG-Based co-contraction also increased but followed a smoother and more gradual trajectory. Overall, EMG-Track showed greater time-dependent variation across stance, with pronounced early- and late-stance elevations and a distinct mid-stance reduction. In contrast, EMG-Based co-contraction remained more evenly distributed across the stance (Figure 1).

In early stance, no significant three-way interaction was observed between Footwear, Method, and Speed ($F_{(2,34)}$=1.504, p=0.237, η_g^2=0.004). The Footwear and Method interaction ($F_{(2,34)}$=0.765, p=0.473, η_g^2=0.004) and the interaction between Method and Speed ($F_{(1,17)}$=0.765, p=0.249, η_g^2=0.003) were also not significant. Despite the lack of significant interactions, there was a significant main effect of Method ($F_{(1,17)}$=27.261, p=0.001, η_g^2=0.301) with higher co-contraction observed in the EMG-Track method compared to the EMG-Based method (p<0.001) (Figure 1) (see Table 1).

During mid-stance, the three-way interaction between Footwear, Method, and Speed was not significant ($F_{(2,34)}$=1.913, p=0.163, η_g^2=0.003). A significant interaction was found between Footwear and Method ($F_{(2,34)}$=18.788, p<0.001, η_g^2=0.045). EMG-Track showed lower co-contraction compared to EMG-Based for LPR (p<0.001), MPR (p<0.001), and NR (p<0.001). No differences were observed across the footwear conditions for the EMG-Based method. In contrast, EMG-Track comparisons showed differences across footwear with higher co-contraction between LPR versus MPR (p<0.001) and NR (p<0.001). The interaction between Method and Speed was not significant ($F_{(2,34)}$=0.788, p=0.862, η_g^2=0.002). Although it was dependent on the interaction, there was a significant main effect of Method ($F_{(1,17)}$=54.00, p<0.001, η_g^2=0.363) with the EMG-Track method showing lower co-contraction compared to the EMG-Based method (p<0.001) (Figure 1) (see Table 2).

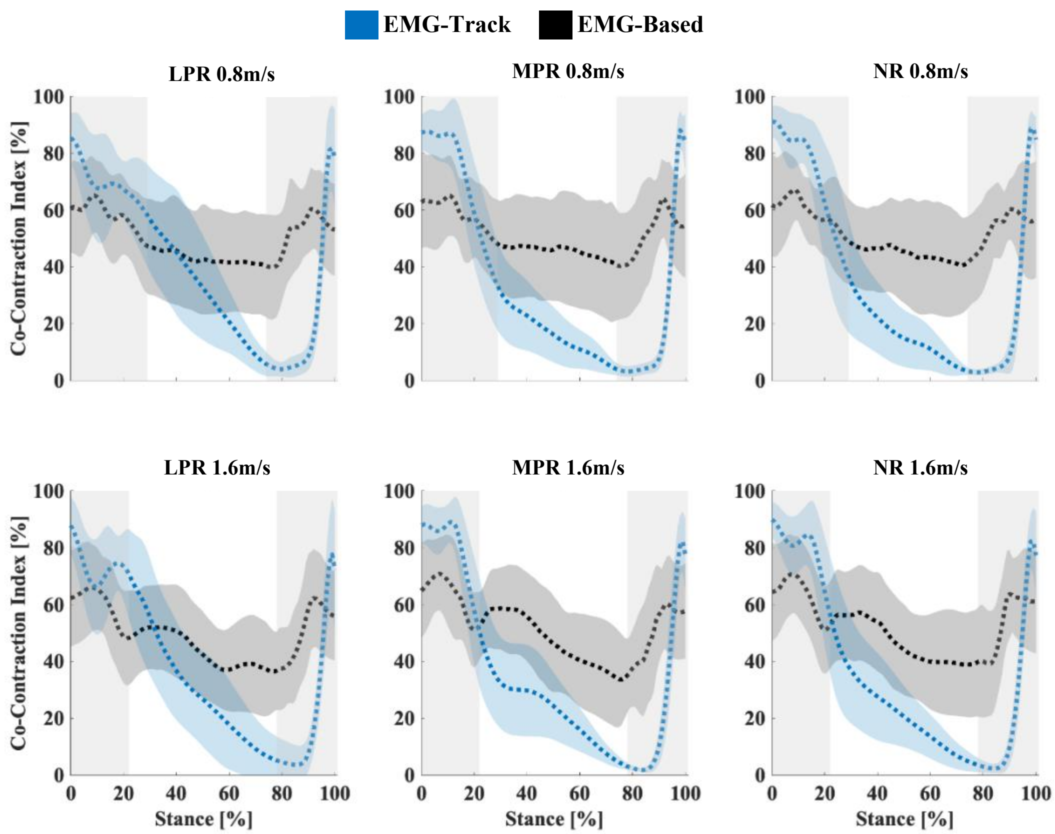

Figure 1: Time-varying co-contraction index between the peroneus longus and tibialis anterior during the stance phase across three footwear conditions (LPR, MPR, NR) and two walking speeds (0.8 m/s and 1.6 m/s). Blue lines represent co-contraction based on muscle moments (EMG-Track), while black lines represent co-contraction based on EMG (EMG-Based). Shaded areas indicate variability (± standard deviation). Each condition's stance phase is divided into early, mid, and late stances. Grey areas indicate early and late stance; the white area indicates midstance.

Table 1: Early Stance PL/TA Averaged Co-contraction

Footwear	Method	Speed	Mean Co-contraction	SD Co-contraction
LPR	EMG-Based	0.8	58.2	12.0
	EMG-Track		69.9	8.08
	EMG-Based	1.6	60.5	11.4
	EMG-Track		73.5	10.5
MPR	EMG-Based	0.8	59.0	11.9
	EMG-Track		71.1	14.0
	EMG-Based	1.6	64.0	11.8
	EMG-Track		81.4	7.19
NR	EMG-Based	0.8	59.4	10.5
	EMG-Track		74.7	8.99
	EMG-Based	1.6	64.4	11.2

	EMG-Track		81.9	6.63

Abbreviations: PL, peroneus longus; TA, tibialis anterior; LPR, lateral-posterior ridge; MPR, medial-posterior ridge; NR, no ridge; SD, standard deviation.

Table 2: Mid Stance PL/TA Averaged Co-contraction

Footwear	Method	Speed	Mean Co-contraction	SD Co-contraction
LPR	EMG-Based	0.8	43.3	19.3
	EMG-Track		31.5	14.9
	EMG-Based	1.6	43.7	15.1
	EMG-Track		30.7	14.0
MPR	EMG-Based	0.8	45.9	20.2
	EMG-Track		16.8	18.8
	EMG-Based	1.6	47.5	14.6
	EMG-Track		23.9	10.4
NR	EMG-Based	0.8	45.0	18.8
	EMG-Track		17.2	9.71
	EMG-Based	1.6	47.0	16.3
	EMG-Track		23.8	10.5

Abbreviations: PL, peroneus longus; TA, tibialis anterior; LPR, lateral-posterior ridge; MPR, medial-posterior ridge; NR, no ridge; SD, standard deviation.

Peroneus Longus/Gastrocnemius Medialis (PL/MG) Muscle Pair

For the PL/MG muscle pair, EMG-Track co-contraction produced lower values than EMG-Based during early stance, with EMG-Based showing higher and more sustained values immediately after initial contact (Figure 2). As stance progressed toward mid-stance, the difference between methods diminished, with the EMG-Track and EMG-Based curves converging and, in some portions of mid-stance, partially overlapping. During this phase, both methods demonstrated relatively similar magnitudes and temporal profiles compared to early stance. Overall, EMG-Track showed greater temporal variation during stance, whereas EMG-Based co-contraction exhibited a smoother, more sustained pattern over time (Figure 2).

A significant three-way interaction between Footwear, Method, and Speed was observed ($F_{(2,34)}=6.779$, $p=0.003$, $\eta_g^2=0.020$), indicating that the effect of co-contraction method depends on footwear and walking speed. Post-hoc two-way ANOVAs for Footwear and Method were performed separately at different speeds. At 0.8 m/s, there was a significant Footwear and Method interaction effect ($F_{(2,34)}=21.617$, $p<0.001$, $\eta_g^2=0.113$). No differences in co-contraction were observed between LPR EMG-Track versus EMG-Based, but this approached significance with higher co-contraction in EMG-Based versus EMG-Track ($p=0.006$). Lower co-contraction was found for EMG-Track versus EMG-Based for MPR ($p<0.001$) and NR ($p<0.001$). No differences were observed for the EMG-Based method between the footwear comparisons. For EMG-Track, higher co-contraction was observed in LPR versus MPR ($p<0.001$) and NR ($p<0.001$). At 1.6 m/s, the Footwear and Method interaction effect was also significant ($F_{(1.47,24.98)}=4.933$, $p=0.024$, $\eta_g^2=$ 0.021). Lower co-contraction was observed for EMG-Track versus EMG-Based for LPR ($p<0.001$), MPR ($p<0.001$), and NR ($p<0.001$). For EMG-Track across footwear conditions, higher co-contraction was observed for LPR versus MPR ($p<0.001$) and versus NR ($p<0.001$). For all footwear comparisons in EMG-Based, no differences were observed.

Additionally, two-way ANOVAs for Speed and Method were performed at each level of Footwear (LPR, MPR, NR). In LPR, there was a significant interaction effect between Method and Speed, ($F_{(1,17)}=17.970$, $p<0.001$, $\eta_g^2=0.054$). In the LPR condition, the EMG-Track showed higher co-contraction in 0.8 m/s versus 1.6 m/s ($p<0.001$), but these differences were not observed with EMG-Based speed comparisons ($p=0.129$). The post-hoc tests indicated that there were no significant two-way interaction effects between Method and Speed for the MPR ($F_{(1,17)}=1.100$, $p=0.309$, $\eta_g^2=0.007$) and NR ($F_{(1,17)}=3.897$, $p=0.0650$, $\eta_g^2=0.021$) conditions. However, a significant main effect for Method was present for MPR ($F_{(1,17)}$=94.502, p<0.001, η_g^2=0.675) and NR ($F_{(1,17)}$=92.618, p<0.001, η_g^2=0.677), with the EMG-Track method showing lower co-contraction compared to the EMG-Based method (p<0.001) (Figure 2) (see Table 3).

In midstance, the three-way interaction between Footwear, Method, and Speed was not significant, ($F_{(2,34)}$=0.411, p=0.666, η_g^2=0.001). A significant interaction was found between Footwear and Method ($F_{(2,34)}$=11.343, p<0.001, η_g^2=0.026). No differences were observed in co-contraction between EMG-Track versus EMG-Based for LPR, but this approached significance with lower co-contraction in EMG-Track versus EMG-Based (p=0.038). Lower co-contraction was observed for MPR EMG-Track versus EMG-Based for MPR (p<0.001) and NR EMG-Track versus EMG-Based for NR (p<0.001). No differences between footwear were observed for the EMG-Based method; however, EMG-Track revealed higher co-contraction in LPR versus MPR (p<0.001) and NR versus MPR (p<0.001). A significant interaction was also found between Method and Speed ($F_{(2,34)}$=0.411, p<0.001, η_g^2=0.038). No differences in co-contraction were observed between EMG-Track and EMG-Based at 0.8 m/s, but this approached significance with higher co-contraction in EMG-Based (p=0.0210). EMG-Track, however, had significantly lower co-contraction than EMG-Based at 1.6 m/s (p<0.001). No differences were observed in the EMG-Track comparison for speeds (p=0.410). EMG-Based showed higher co-contraction for 1.6 m/s versus 0.8 m/s (p<0.001).

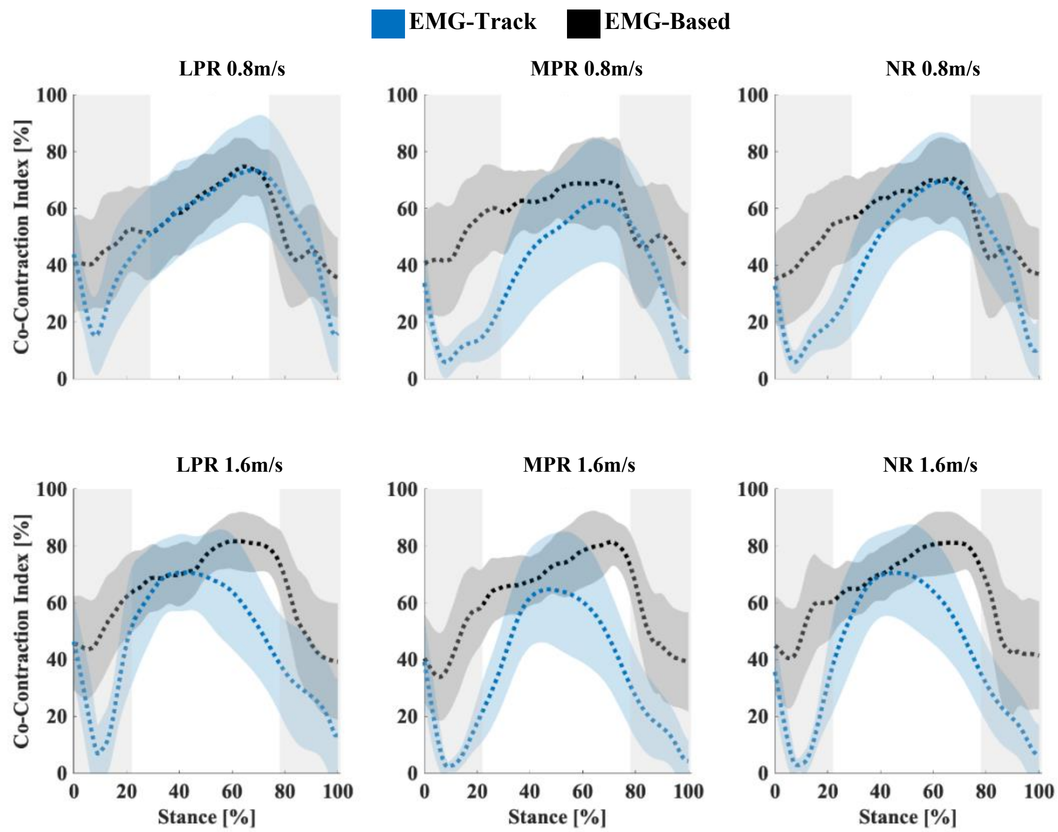

Figure 2: Time-varying co-contraction index between the peroneus longus and gastrocnemius medialis during the stance phase across three footwear conditions (LPR, MPR, NR) and two walking speeds (0.8 m/s and 1.6 m/s). Blue lines represent the EMG-Track method, while black lines represent the EMG-Based method. Shaded areas around the traces indicate the standard deviation. The stance phase is divided into early, mid, and late stance for each condition. Grey areas are the early and late stance whereas the white area indicates midstance.

Table 3: Early Stance PL/MG Averaged Co-contraction

Footwear	**Method**	**Speed**	**Mean Co-contraction**	**SD Co-contraction**
LPR	EMG-Based	0.8	46.5	16.4
	EMG-Track		33.6	12.6
	EMG-Based	1.6	51.7	14.6
	EMG-Track		25.2	11.6
MPR	EMG-Based	0.8	49.3	17.0
	EMG-Track		14.6	5.59
	EMG-Based	1.6	43.8	14.7
	EMG-Track		12.9	4.99
NR	EMG-Based	0.8	45.4	14.9
	EMG-Track		16.6	5.45
	EMG-Based	1.6	50.0	14.6
	EMG-Track		14.9	6.05

Abbreviations: PL, peroneus longus; MG, medial gastrocnemius; LPR, lateral-posterior ridge; MPR, medial-posterior ridge; NR, no ridge; SD, standard deviation.

Table 4: Mid-Stance PL/MG Averaged Co-contraction

Footwear	Method	Speed	Mean Co-contraction	SD Co-contraction
LPR	EMG-Based	0.8	65.2	10.3
	EMG-Track		64.6	15.5
	EMG-Based	1.6	74.4	7.54
	EMG-Track		61.2	13.8
MPR	EMG-Based	0.8	64.5	11.0
	EMG-Track		50.4	18.7
	EMG-Based	1.6	72.1	9.09
	EMG-Track		50.8	16.0
NR	EMG-Based	0.8	65.3	9.47
	EMG-Track		57.1	13.9
	EMG-Based	1.6	73.0	8.86
	EMG-Track		58.6	14.4

Abbreviations: PL, peroneus longus; MG, medial gastrocnemius; LPR, lateral-posterior ridge; MPR, medial-posterior ridge; NR, no ridge; SD, standard deviation.

Peroneus Longus/Soleus (PL/SOL) Muscle Pair

For the PL/SOL muscle pair, EMG-Track co-contraction was markedly lower than EMG-Based throughout early stance, with EMG-Based values consistently higher immediately after initial contact (Figure 3). During this early portion of stance, EMG-Track increased gradually but remained substantially below EMG-Based values. As early stance progressed into mid-stance, the difference between methods diminished, with the EMG-Track and EMG-Based curves becoming more similar in magnitude and, in some portions of mid-stance, partially overlapping. During this phase, both methods showed relatively stable co-contraction profiles compared with early-stance levels. Overall, EMG-Track showed greater temporal modulation across stance, with lower early-stance values and convergence during mid-stance. In contrast, EMG-based co-contraction exhibited a smoother, more sustained pattern over time (Figure 3).

In early stance, a significant three-way interaction between Footwear, Method, and Speed was observed ($F_{(2,34)}=3.811$, $p=0.032$, $\eta_g^2=0.009$). We performed Footwear and Method ANOVAs at each Speed level to assess how methods influenced co-contraction across footwear conditions at different speeds. At 0.8 m/s, there was a significant Footwear and Method interaction effect ($F_{(2,34)}=19.448$, $p<0.001$, $\eta_g^2=0.103$). Lower co-contraction was found for EMG-Track versus EMG-Based for LPR ($p=0.002$), MPR ($p<0.001$) and NR ($p<0.001$). No differences were observed for the EMG-Based footwear comparisons. In contrast, for EMG-Track, higher co-contraction was observed in LPR versus MPR ($p<0.001$) and versus NR ($p<0.001$), and NR versus MPR ($p<0.001$). At 1.6 m/s, there was a significant interaction between Footwear and Method ($F_{(2,34)}=8.130$, $p=0.001$, $\eta_g^2=0.028$). Lower co-contraction was observed for EMG-Track versus EMG-Based for LPR ($p<0.001$), MPR ($p<0.001$) and NR ($p<0.001$). No differences between footwear conditions were observed for EMG-Based. However, for EMG-Track, higher co-contraction was observed across different footwear conditions, namely LPR versus MPR ($p<0.001$) and versus NR ($p<0.001$), and NR versus MPR ($p<0.001$).

Additionally, post-hoc two-way Method and Speed ANOVAs were performed at each level of Footwear (LPR, MPR, NR). In LPR, there was a significant Method and Speed interaction effect ($F_{(1,17)}=12.977$, $p=0.002$, $\eta_g^2=0.076$). In the LPR condition, EMG-Track showed higher co-contraction at 0.8 m/s versus 1.6 m/s ($p=0.005$), but these differences were not observed in the EMG-Based comparison for speeds ($p=0.094$). The post-hoc tests indicated that there were no significant two-way interaction effects between Method and Speed for the MPR ($F_{(1,17)}=3.941$, $p=0.0640$, $\eta_g^2=0.014$) and NR ($F_{(1,17)}=3.111$, $p=0.0960$, $\eta_g^2=0.012$) conditions. However, a significant main effect for Method was present for MPR ($F_{(1,17)}=86.363$, $p<0.001$, $\eta_g^2=0.712$), and

NR ($F_{(1,17)}$=69.262, p<0.001, η_g^2=0.695), with the EMG-Track method showing lower co-contraction values compared to the EMG-Based method (p<0.001) (Figure 3) (see Table 5).

In midstance, there was no significant three-way interaction between Footwear, Method, and Speed ($F_{(2,34)}$=0.393, p=0.678, η_g^2=0.002) as well as no Footwear and Method ($F_{(2,34)}$=2.289, p=0.117, η_g^2=0.009) and no Method and Speed ($F_{(1,17)}$=0.018, p=0.894, η_g^2=0.001) interaction. Additionally, there was no significant main effect for Method ($F_{(1,17)}$=2.701, p=0.119, η_g^2=0.0230) (Figure 3) (see Table 6).

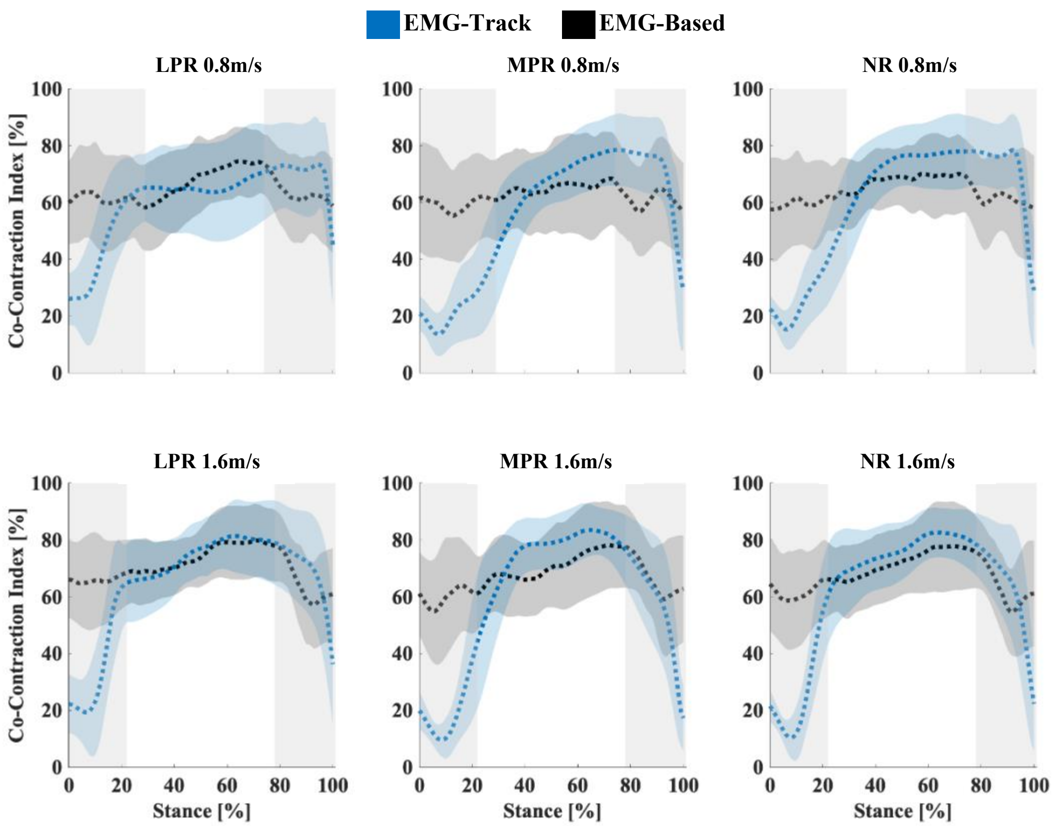

Figure Error! No text of specified style in document.**: Time-varying co-contraction index between the peroneus longus and soleus during the stance phase across the footwear conditions (LPR, MPR, NR) and speeds (0.8 m/s and 1.6 m/s).** Blue lines represent co-contraction predicted through EMG-Track, while black lines represent co-contraction predicted through EMG-Based. Shaded areas around the co-contraction traces indicate variability (± standard deviation). The stance phase is divided into early, mid, and late stance for each condition. Grey areas indicate early and late stance; white area indicates midstance.

Table 5*:*Early Stance PL/SOL Averaged Co-contraction

Footwear	Method	Speed	Mean Co-contraction	SD Co-contraction
LPR	EMG-Based	0.8	61.4	15.2
	EMG-Track		44.5	13.1
	EMG-Based	1.6	65.5	13.6
	EMG-Track		34.6	12.3
MPR	EMG-Based	0.8	59.1	14.0
	EMG-Track		23.2	9.91
	EMG-Based	1.6	59.7	16.7
	EMG-Track		18.8	8.01
NR	EMG-Based	0.8	60.4	14.1
	EMG-Track		28.1	9.21
	EMG-Based	1.6	61.4	14.4
	EMG-Track		23.8	7.91

Abbreviations: PL, peroneus longus; SOL, soleus; LPR, lateral-posterior ridge; MPR, medial-posterior ridge; NR, no ridge; SD, standard deviation.

Table 6: Mid-Stance PL/SOL Averaged Co-contraction.

Footwear	Method	Speed	Mean Co-contraction	SD Co-contraction
LPR	EMG-Based	0.8	68.4	12.3
	EMG-Track		65.4	13.4
	EMG-Based	1.6	74.5	11.2
	EMG-Track		74.3	8.72
MPR	EMG-Based	0.8	65.1	15.5
	EMG-Track		66.8	6.64
	EMG-Based	1.6	70.4	15.0
	EMG-Track		73.9	7.05
NR	EMG-Based	0.8	68.0	9.76
	EMG-Track		72.5	7.86
	EMG-Based	1.6	71.8	13.0
	EMG-Track		74.8	7.36

Abbreviations: PL, peroneus longus; SOL, soleus; LPR, lateral-posterior ridge; MPR, medial-posterior ridge; NR, no ridge; SD, standard deviation.

DISCUSSION

This study compared two co-contraction indices, finding significant differences between the more conventional co-contraction analysis (i.e., EMG-Based) and a novel moment-based co-contraction index (i.e., EMG-Track) when walking in three footwear conditions and two walking speeds. Additionally, EMG-Track was more sensitive at detecting differences in co-contraction across all footwear conditions using three muscle pairs: PL/TA, PL/MG and PL/SOL. We selected the PL/TA muscle pair because it is frequently used in the literature and plays a prominent role in mediolateral stability[40-42]. Although used to a lesser extent than PL/TA, the PL/MG and PL/SOL pairs were also included due to their use in prior studies assessing co-contraction during walking[43,44]. These pairs are especially relevant because at the subtalar joint, they possess supination moment arms during foot pronation and pronation moment arms during foot supination[45], which may inform their roles in maintaining mediolateral stability. To our knowledge, this is the first study to use subtalar-joint muscle moments to evaluate co-contraction, providing insight into how co-contraction stabilizes the subtalar joint during walking on mediolaterally uneven surfaces.

Consistent with our first hypothesis, EMG-Track better captured differences in co-contraction across unstable footwear conditions. The PL/MG, PL/SOL, and PL/TA muscle pairs all showed differences between footwear conditions in either early or mid-stance, while EMG-Based failed to detect any differences. There are a few possible reasons why EMG-Track was more sensitive to detecting changes compared to the EMG-Based method. First, muscle force depends on fiber length and contraction velocity, meaning force output can vary even when EMG activity remains unchanged[16-18,49]. For example, Maharaj *et al.* (2019) found that tibialis anterior shortened throughout the stance phase despite relatively constant EMG activity at both slow and fast walking speeds[50]. The importance of a muscle's intrinsic properties during mediolateral perturbations was highlighted by John et al. (2013), who showed that removing intrinsic muscle properties increased the cumulative deviation in lower-limb joint angles from 9.1° to 23.0° during a forward dynamics simulation[51]. Also, EMG alone may not entirely explain how muscles control whole-body stability during locomotion[51]. Second, unstable footwear conditions alter the way ground reaction forces are applied to the foot, thereby influencing the joint moments required to stabilize the foot. For instance, the LPR condition causes additional pronation during early and mid-stance, thereby altering the muscle forces required to stabilize the subtalar joint. A muscle moment-based method may be more sensitive to these mechanical effects, while an EMG-based method may not capture these specific, subtle effects of external forces, as muscle force may change through other mechanisms without altering electrical activity[49, 52].

The EMG-Track method was also more sensitive to changes in walking speed. For PL/SOL and PL/MG, co-contraction was lower in EMG-Track than in EMG-Based under MPR and NR conditions. In the LPR condition, EMG-Track showed significantly higher co-contraction at 0.8 m/s than at 1.6 m/s, while EMG-Based showed no differences. This aligns with studies showing higher co-contraction at slower speeds in shank and thigh muscles[22,53]. Slower speeds may require greater co-contraction due to the longer stance phase, thereby increasing the duration of foot and ankle instability[22,53]. Additionally, EMG-Track traces exhibited sharper increases and decreases in co-contraction at higher speeds, reflecting quicker adjustments in muscle co-contraction[22,53]. While further analysis is needed to confirm this, it may support the idea that EMG-Track is more sensitive to the increased need for subtalar joint stabilization at different speeds[22,53]. To add, as walking speed increases, the foot-ankle joint complex faces greater loads[54,55]. At faster speeds, the ankle joint may shift some stabilization demands to more proximal muscles[53,54], reducing unnecessary involvement of distal muscles during high-speed or prolonged activities. Notably, EMG-Track showed no speed-related difference in PL/MG at midstance, whereas EMG-Based showed higher co-contraction at 1.6 m/s. These results could reflect a false-positive difference in

EMG-Based methods, which do not account for muscle moment arms or function during stance. Specifically, the MG may have exhibited higher activity, which may primarily contribute to sagittal plane motion via an internal joint moment[45,56,57], and, therefore, may not significantly influence its supination muscle moment at the subtalar joint, which would be reflected in the EMG-Track method and not the EMG-Based method. Additionally, the triceps surae muscles have greater effective moment arms about the ankle joint than about the subtalar joint[45]. This highlights the need for moment-based approaches, as EMG-based methods ignore joint-specific mechanics such as varying moment arms.

Consistent with our second hypothesis, we found significant differences in co-contraction magnitude across methods. Specifically, the analysis showed that the EMG-Track method consistently reported lower co-contraction than the EMG-Based method. Similar to previous studies[58] and for most of our results, co-contraction estimated by EMG-Track was significantly lower than that measured by EMG-Based[58]. It is important to note that the EMG-Track method constrained patterns of muscle excitations to experimental EMG. Therefore, the differences between the two methods may be explained in part by the constraints on muscle force to match the overall internal joint moment[38,59]. For instance, a muscle's force is highly dependent on its length, so force-producing capacity decreases at shorter or longer lengths even if EMG activity remains high. Furthermore, fewer cross-bridges are attached at faster contraction velocities at a given time, decreasing force output[17,18,60]. Additionally, EMG signals represent the summation of motor unit action potentials, which are prone to amplitude cancellation and superposition[61]. While muscle excitations do precede muscle force generation, they are not an indicator of the relative contribution of each muscle to the joints it crosses. Muscles of the shank, which span multiple joints, exhibit complex mechanical behaviours due to their multiple moment arms relative to joints with different degrees of freedom[62]. Therefore, despite differences in excitation levels, the mechanical output can vary depending on how these muscles interact across joints.

EMG-based methods produced higher co-contraction values than EMG-Track and failed to detect differences across uneven foot position conditions. These findings support concerns about surface EMG's limitations in detecting actual co-contraction differences. DaSilva *et al.* (2021) and Holcomb *et al.* (2022) found no differences in ankle or knee co-contraction between even and uneven surfaces[10,63] Challenges in detecting co-contraction in these younger adult participants was suggested to arise from the authors' inability to replicate real-world uneven surfaces[10,63]. Our study similarly used simulated surfaces, but the phase-specific significant differences in co-contraction we observed with EMG-Track suggest that the method for detecting co-contraction matters more than the nature of the surface.

Differences between co-contraction estimates derived from EMG-Track and EMG-based indices may furthermore affect the interpretation of co-contraction. For instance, persons with chronic ankle instability have reduced muscle strength[64] and variable levels of muscle excitations[40,65,66]. EMG-based estimates suggest that increased co-contraction may be needed to stabilize the ankle joint[40,67] in these populations and that, therefore, a lack of co-contraction may require interventions to optimize excitations[40]. However, a muscle moment-based co-contraction index may yield different results and suggest that the muscles are not generating sufficient force for stability, thereby increasing the risk of reinjury[64]. Conversely, studies have suggested that high co-contraction leads to joint damage[68]. However, muscle force estimates of co-contraction are better predictors of joint deterioration, as they reflect the joint's mechanical load[29]. EMG-Track's greater sensitivity may explain prior studies that reported no co-contraction differences despite changing stability demands.

Several limitations should be noted when interpreting this work's results. First, simulated muscle forces are challenging to validate *in vivo*, though we incorporated physiological constraints to make the simulations more realistic with respect to a person's physiology. Second, model simplifications, such as omitting tendon compliance for the thigh muscles, were made for convergence but are unlikely to affect key outcomes[38,59]. Regarding how co-contraction was calculated, we chose a modification of the Falconer and Winter (1985) method rather than the Rudolph *et al.* (2000) method, which has been shown to correlate more closely with joint quasi-stiffness[21,69,70]. If we opted for the Rudolph *et al.* (2000) method, muscle moments would need to be normalized, since without normalization, there would be no upper limit to co-contraction, which could produce exceptionally high values[70]. Normalizing muscle moments would ultimately influence the maximal muscle force input from our modelled muscle force[58], which is crucial for representing muscle properties during co-contraction. For instance, the muscle moment produced by the plantarflexors is four times greater than that produced by the dorsiflexors, and these differences, from our perspective, need to be captured in this analysis[15,71]. Additionally, we normalized EMG to the maximum value in our task, as in previous studies[7,58], because obtaining maximum voluntary contractions for each muscle before testing is impractical[72].

In conclusion, the EMG-Track method was more sensitive than the traditional EMG-based method for calculating muscle-pair co-contraction, and it proved more effective at detecting differences across unstable conditions and at varying speeds. This approach is novel in two key ways: first, it uses a dynamic optimization framework constrained by EMG to incorporate muscle physiology; and second, it uses subtalar joint muscle moments to compute co-contraction that stabilizes the joint during mediolateral perturbations. By integrating EMG patterns to estimate muscle forces and joint moments, this hybrid method offers a more comprehensive understanding of joint stabilization, accounting for factors such as force-length and force-velocity relationships, activation dynamics, and muscle-tendon properties. The observed differences in co-contraction using the EMG-Track method may be important for understanding co-contraction in other populations with foot stability issues (e.g., older adults, individuals with chronic ankle instability). These interpretations would inform rehabilitation programs that aim to optimize muscle function in these conditions by increasing or decreasing co-contraction through training or biofeedback (e.g., running gait simulators).

METHODS

Participants

Eighteen young adult participants (9 females and 9 males; Body Mass: 80.17kg ± 12.69; Age: 22.78 ± 1.73) were recruited from the local community to participate in this study. Individuals were screened via phone or email interview, and eligible participants were further screened in person for self-reported lower-limb musculoskeletal injuries or pathologies.. Exclusion criteria for all subjects included any lower-limb pathology (e.g., ligament, muscle, joint, or tendon injury, neurological impairment, and/or painful foot/ankle)[16,73]. All experimental procedures were reviewed and approved by the University of Calgary Conjoint Health Research Ethics Board (CHREB) (Ethics ID: REB23-0634). All methods were carried out in accordance with the relevant guidelines and regulations set by the CHREB and the Tri-Council Policy Statement: Ethical Conduct for Research Involving Humans (TCPS2). Voluntary informed written consent was obtained from all participants prior to participation in the study.

Experimental Protocol and Footwear Conditions

Participants walked on a force-instrumented split-belt treadmill (Bertec, Columbus, OH, USA) at a slow (0.8 m/s) and fast (1.6 m/s) walking speed under the following three footwear conditions: 1) 1 cm half-ridge located on the medial-posterior aspect of the outsole, known as the medial posterior ridge (MPR) condition, 2) 1 cm half-ridge located on the lateral-posterior aspect of the outsole, known as the lateral posterior ridge (LPR) condition and 3) no ridge conditions (NR) (Figure 4). The footwear conditions were 3D-printed and designed (SOLIDWORKS, Dassault Systèmes, France) so that the MPR condition limited pronation, and the LPR condition caused additional pronation. The footwear conditions were printed in US men's sizes 5, 7, 9, and 11.

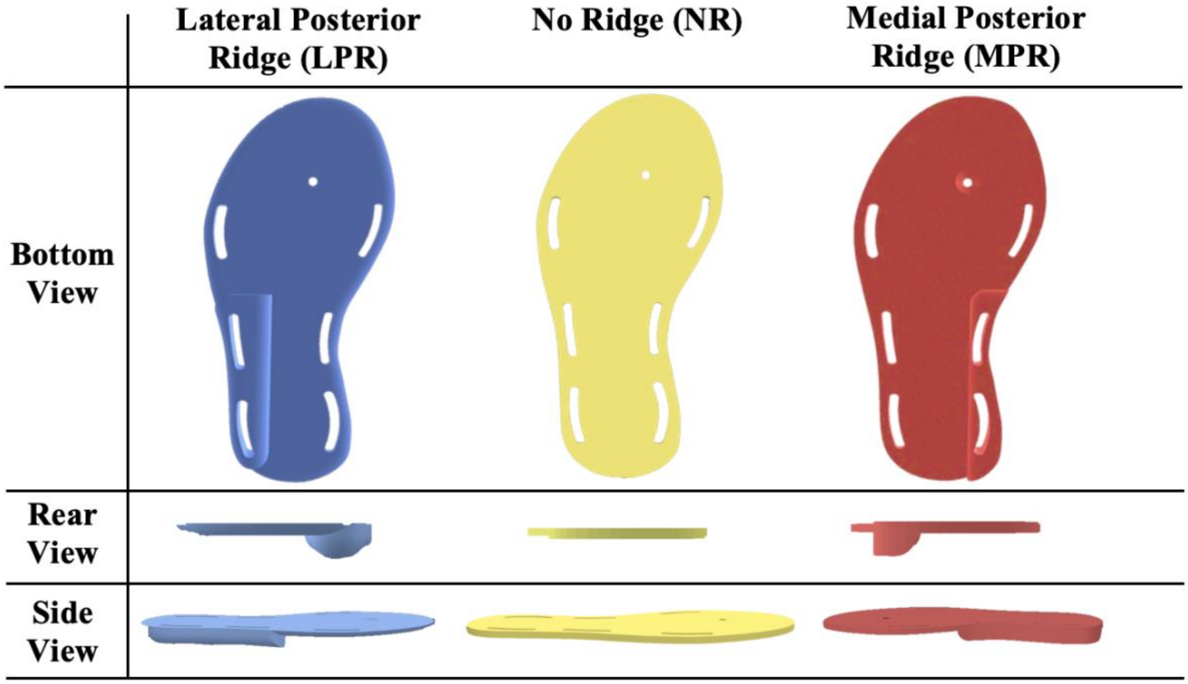

Figure 4: 3D-printed footwear conditions designed to manipulate pronation and supination. The red footwear condition features a 1 cm medial-posterior ridge (MPR) to limit pronation. The blue footwear condition includes a 1 cm lateral-posterior ridge (LPR) to increase pronation. The yellow footwear condition serves as the control with no ridge (NR). Each footwear condition is shown for three perspectives: bottom view, rear view and side view. For the side view, LPR and NR conditions are displayed from the lateral side, and MPR is displayed from the medial side.

Participants wore a 3D-printed sole, which was secured to the foot using elastic shoelaces (Stepace)[74]. Data collection lasted for 20 seconds per trial. A pseudorandom counterbalanced experimental design was utilized to reduce the effects of condition order (Researcher Randomizer). Using custom 3D-printed footwear eliminates inter-subject variability caused by different shoe and insole types, as varying insole stiffness and footwear can significantly alter joint kinematics and spatiotemporal gait parameters[75].

Kinematics and Kinetics

30 reflective markers, each 12.5 mm in diameter, were placed over body landmarks and tracked using a 12-camera motion capture system (Qualysis, Gothenburg, Sweden) at 240 Hz. The markers were placed on the right lower limb of the participants as follows: pelvis markers were placed on the right and left anterior superior iliac spine and posterior iliac spine; thigh markers were placed on the greater trochanter, medial and lateral epicondyle of the femur, along with a cluster of 4 markers on the lateral and anterior aspect of the thigh; shank markers were placed on medial and lateral malleoli, along with a cluster of 4 markers on the anterior and lateral aspect of the shank; foot markers were placed on the 1st, 3rd, and 5th digits, the 1st, 2nd, and 5th metatarsal heads, the 1st, 2nd, and 5th metatarsal base, the medial, lateral, and distal aspects of the calcaneus, and on the navicular tuberosity[91].

Three-dimensional ground reaction forces applied to the left and right feet during walking were determined using the force-instrumented split-belt treadmill at a sampling frequency of 2400 Hz. Participants walked on the treadmill with the right and left feet on the right and left belts, respectively. Ensuring the two feet contacted separate belts allowed the 3D forces and moments to be calculated separately for the right and left legs. If the participant stepped on the same belt with both feet in a single gait cycle, those steps were removed from the analysis. Ground reaction force data was also used to determine subphases of stance: early, mid and late stance (Figure 5)[68].

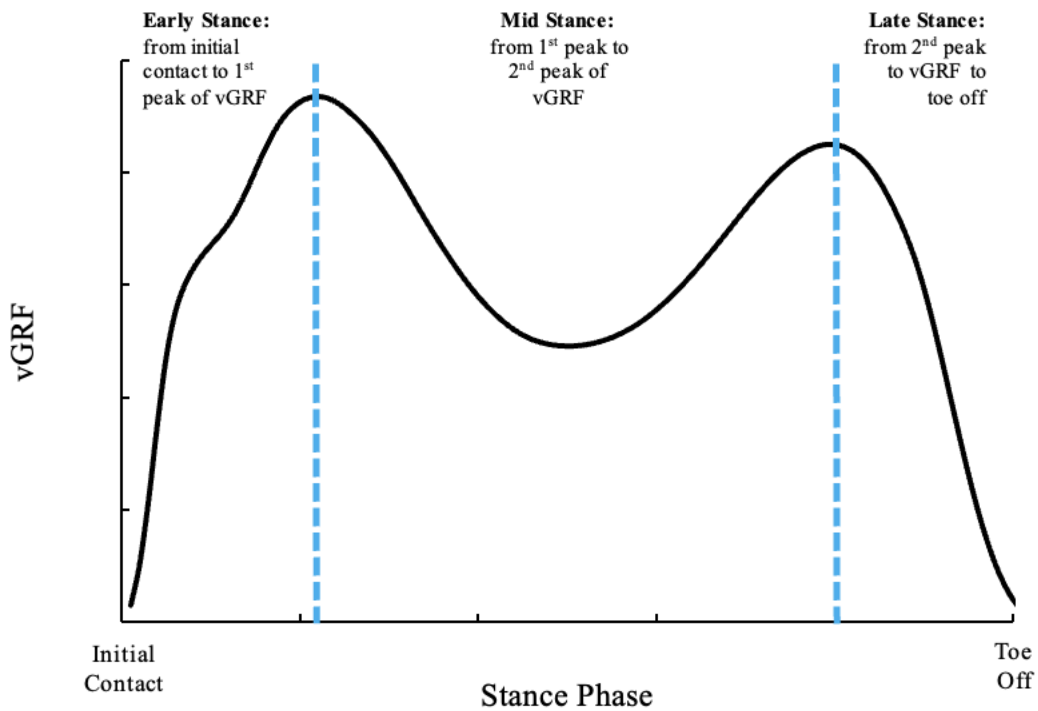

Figure 5: Phases of stance defined based on the peaks of the vertical ground reaction forces (vGRF). Adapted from Thoma et al. (2016).

Electromyography

EMG activity was measured with surface electrodes using a wireless system (Delsys Trigno, Natick, MA, USA). Accurate skin preparation (abraded and cleaned with alcohol wipes) was used to reduce baseline noise and skin impedance between the electrode and the source signal. Double-differentiated surface electrodes, with an interelectrode spacing of 10 mm for four electrodes, were placed over the tibialis anterior (TA), soleus (SOL), gastrocnemius medialis (MG), gastrocnemius lateralis (LG), peroneus tertius (PT) and peroneus longus (PL) muscle bellies. The electrodes were secured onto the skin to avoid movement artifacts using BSN Medical Hypafix® Dressing Tape. An external trigger was used to synchronize EMG data to the motion capture system, and the EMG data was sampled at a rate of 4000 Hz.

Musculoskeletal Modelling

A generic full-body musculoskeletal model proposed by Rajagopal *et al.* (2016) was used. These authors developed the model with 37 degrees of freedom and 80 muscle-tendon units actuating the lower limb, along with 17 torque actuators driving the body (torque-driven)[76]. This generic musculoskeletal model was adjusted to include only the pelvis and the right lower limb[76]. The PT muscle was added using parameters from Maharaj *et al.* (2021)[79]. The mass removed from the segments during model modification was added back to the pelvis mass to ensure the participant's mass remained unchanged. The model included a pelvis that could translate and rotate relative to the ground with 3 degrees of freedom of translation and rotation (6 degrees of freedom total)[76]. The knee was modelled as a 1-degree-of-freedom hinge joint, whereas the ankle, subtalar, and metatarsophalangeal joints were each modelled as 1-degree-of-freedom pin joints. The hip joint was modelled with 3 degrees-of-freedom[76]. The *DeGrooteFregly2016Muscle* model (41 Hill-type muscle-tendon units) was selected because it is continuous and differentiable, which is essential for performing direct collocation to solve optimal control problems[38]. Dynamic optimization accounted for muscle-tendon and activation dynamics, which were enabled for the muscles that would control the foot, specifically the ankle and subtalar joints (i.e., SOL, LG, MG, TA, PL, PT, tibialis posterior, peroneus brevis, flexor hallucis longus, flexor digitorum longus, extensor hallucis longus, extensor digitorum longus).

Data Analysis

Kinetics and Kinematics

Before computing 3D kinetics and kinematics, a static trial was used to scale the *OpenSim* model to each participant's mass, height, and marker-based segment lengths using calculated scale factors[80]. After scaling, the locations of model markers were moved to match the location of the experimental markers obtained using the motion capture system[80]. The scaled model was used for all subsequent analyses for each participant, using participant-specific musculoskeletal models[80].

Raw force plate and motion capture data were analyzed with a custom MATLAB script (R2023b; MathWorks, Inc.). Force plate and marker position data were low-pass filtered using a dual-pass second-order (i.e., zero-lag, 4th order) Butterworth filter with a cut-off frequency of 15 Hz[81,82]. Inverse kinematics was performed on the marker data to estimate joint angles using a global optimization scheme that computes the joint angles that minimize errors between experimental and model markers[83]. The inverse kinematics routine was implemented using *OpenSim's* methods and cost functions, while we customized the weighting of specific markers for our purposes[83].

Electromyography

EMG data were filtered using a dual-pass, second-order Butterworth bandpass filter between 10 and 500 Hz[7,15,84]. The signal was then rectified and low-pass filtered using an additional dual-pass second-order Butterworth filter (i.e., zero-lag, 4th order) with a 6 Hz cut-off frequency to obtain a linear envelope [7,15,84]. The EMG data was normalized to the maximum amplitude recorded in the walking trials[7,15,84].

Solving the Muscle Redundancy Problem: EMG-Constrained Optimization

To resolve the individual muscle forces responsible for generating the internal joint moments, a dynamic optimization scheme, specifically direct collocation, was used[38,59]. Direct collocation solves for controls (i.e., muscle excitations) and states (i.e., muscle activations, forces) given the musculoskeletal model, kinematics, and ground reaction forces that are constrained to the muscle contraction and activation dynamics[38,59]. We utilized the *OpenSim Moco* framework, which assisted in converting the muscle redundancy problem into an optimal control problem (see

Optimization Procedures) [38,59]. We added an additional term to the cost function, which allowed the optimization to minimize the difference between experimental EMG data and predicted muscle excitations[38,59]. Therefore, we obtained a multi-objective cost function which minimized the sum of squared controls, being the muscle excitations and the weighted reserve actuators[38,59]. Additionally, there was a weighted sum of the difference between predicted muscle excitations and experimental EMG[38,59]:

$$\int_{t_0}^{t_f} \left(\sum_{m=1}^{M} e_m^2 + w_1 \sum_{k=1}^{K} e_R^2 + w_2 \sum_{me=1}^{ME} |e_{me} - EMG_{me}| \right) dt \qquad (\mathbf{1})$$

where, t_0 and t_f were the initial and final times of the movement trajectory, $m = 1, \dots, M$ were the different muscles in the model, $me = 1 \dots, ME$ were the muscles recorded experimentally, $k = 1, \dots, K$ were the various degrees of freedom of the model, e_m was the muscle excitations of each muscle, e_R^2 was the reserve actuators squared at each degree-of-freedom, e_{me} was the predicted muscle excitations for the muscles that were recorded experimentally with EMG, EMG_{me} represented the EMG results obtained experimentally, w_1 was the weight penalizing the use of the reserves since they were non-physiological, and w_2 was the weight determining how closely the excitations should match the experimental EMG[38,59]. It is important to note that the third term of the cost function only modifies the excitations of muscles that had surface EMG recordings[38,59].

There were many constraints on the system as described in detail elsewhere[38,59], and only a few relevant constraints will be discussed. Excitations were bound between 0.001 and 1, where 0.001 was the minimum possible muscle excitation and 1 was the maximal excitation[38,59]:

$$0.001 \leq e_m \leq 1 \qquad (\mathbf{2})$$

Since activation dynamics were included in the system, the activation time constant was 15 ms, and the deactivation time constant was 60 ms[38,59]. Activations were also bound between 0.001 and 1, where 0.001 was the minimum possible muscle activation and 1 was the maximal activation[38,59]:

$$0.001 \le a \le 1 \tag{3}$$

Since reserve actuators were permitted in the model and, in addition to their minimization in the cost function, their torque outputs were constrained to range between -5 and 5 Nm:

$$-5 \le e_R \le 5 \tag{4}$$

When muscle forces are computed at each time point, they must satisfy the internal joint moment constraint at each collocation point (i.e., mesh point):

$$\sum_{m=1}^{M} (d_{mk} F_{Tm}) + e_R = T_{IDk} \tag{5}$$

where, at each degree-of-freedom, k, the sum of the force along the tendon, F_T, for each muscle, m, multiplied by its corresponding moment arm, d_{mk}, along with the contribution from the reserve actuator e_R at each collocation point, must equal the internal joint moment, T_{IDk}, calculated through inverse dynamics at the same collocation point.

The mesh interval, the interval at which collocation occurs, was set to 0.01 s, per established guidelines for gait analyses[38,59]. In addition, to ensure that experimental EMG matches predicted excitations, scale factors were applied to each muscle. Figure 7 describes the basic workflow for solving the optimization problem.

Optimization Procedures

The optimization problems for all 108 trials were solved using Hermite-Simpson discretization implemented with CasADi[85] and IPOPT[86] (Figure 7). Due to the high computational cost of solving a 20-second interval trial, trials were divided into 6-second intervals, which were then sequentially appended with overlap between successive 1-second time intervals. Constraint and convergence tolerances were set to 1e-3[38]. Optimizations were solved on a 64-core desktop computer with a 2.7–4.5 GHz AMD Ryzen Threadripper PRO 5995WX processor. Each optimization problem was solved in 2 to 10 hours per time interval, depending on the condition.

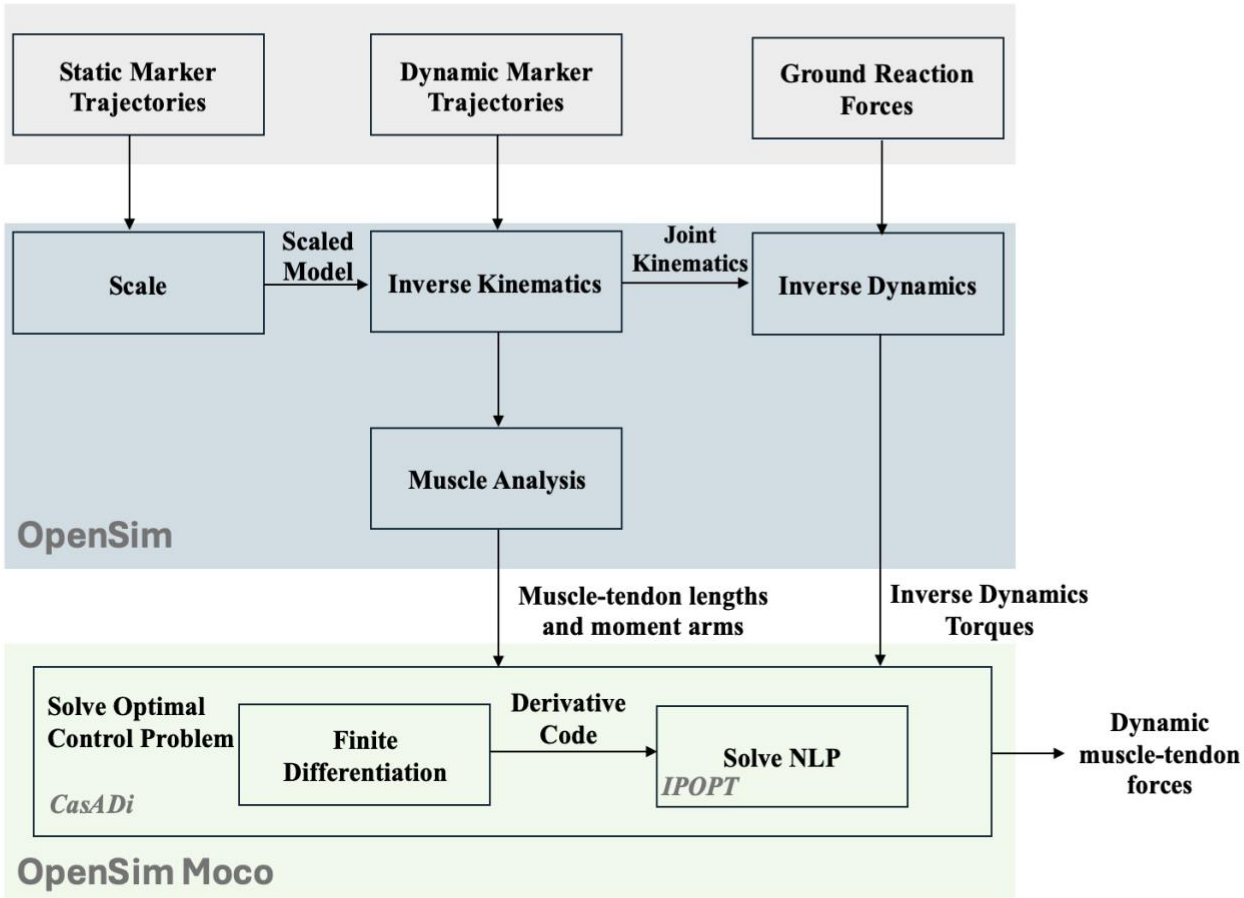

Figure 7: **Overall processing pipeline to solve the muscle redundancy problem.** *OpenSim's* scale, inverse kinematics and inverse dynamics tools were utilized to scale the musculoskeletal model, determine joint kinematics and joint moments, respectively. *OpenSim Moco's* framework was utilized to assist with determining muscle forces. NLP, nonlinear programming. Adapted from De Groote *et al.* (2016).

Determining Co-contraction: "EMG-Track" Co-contraction Index (CCI)

We implemented two versions of co-contraction: EMG-Track and EMG-Based. EMG-Track co-contraction was analyzed in early and mid-stance because this is when co-contraction is necessary to stabilize the foot, and the requirements are likely different in early versus mid-stance. During late stance, the muscles are likely to contribute to toe-off and propulsion. This muscle requirement would be quite different from that for stabilizing the foot during early to mid-ground contact. Antagonistic co-contraction muscle pairs were identified based on their agonist-antagonist relationships at the subtalar joint, as reported in previous literature. The muscle pairs for which co-contraction was calculated were the TA/PL, PL/MG and PL/SOL. The MG and SOL muscles were chosen as several studies have implicated their importance in mediolateral stability[45, 87-89]. The SOL contributes to the mediolateral ankle strategy by shifting the center of pressure laterally[88]. In the neutral position, the Achilles tendon passes medially to the subtalar joint, suggesting, along with the TA, that the MG and SOL contribute to preventing excessive pronation with a small moment arm[89].

Muscle moments were determined as the cross product of the moment arm and muscle force[80]. Muscle moment arms were determined in *OpenSim* as the partial derivative of the change of muscle length over the change in joint angle using the virtual displacement method of the musculoskeletal model[80,90]. EMG-Track co-contraction was then calculated based on the modified method proposed by Falconer and Winter (1985)[69]:

$$CCI = \frac{2\ x\ |Moment\ (t)\ antagonist|}{|Moment\ (t)\ antagonist| + |Moment\ (t)\ agonist|}\ x\ 100\% \qquad (\mathbf{6})$$

where $|Moment\ (t)\ antagonist|$ was the muscle with the lower absolute muscle moment at time point t , and $|Moment\ (t)\ agonist|$ was the muscle with the highest absolute muscle moment at time point t.

Determining Co-contraction: "EMG-Based" Co-contraction Index (CCI)

EMG-Based co-contraction was analyzed in the same phases across the identical pairs of muscles as EMG-Track above. EMG-Based co-contraction was then calculated based on the modified method proposed by Falconer and Winter (1985)[69]:

$$CCI = \frac{2\ x\ EMG\ (t)\ antagonist}{EMG\ (t)\ antagonist + EMG\ (t)\ agonist}\ x\ 100\% \tag{7}$$

where $EMG\ (t)\ antagonist$ was the muscle with the lower EMG at time point t and $EMG\ (t)\ agonist$ was the muscle with the higher EMG at time point t.

Data Processing

All kinetic, kinematic, and EMG measures were time-normalized to 101 data points during stance phase (from right heel strike to right toe-off). Heel strike and toe-off were identified using a 15 N vertical ground reaction force threshold, with heel strike marked when force exceeded 15 N and toe-off when it fell below 15 N. For each participant, all data analysis procedures were performed across 12 steps, and the resulting values for each variable were averaged across steps.

Data Analysis

All statistical analyses were performed using R (Version 2024.04.2+764). A three-way repeated measures ANOVA was performed to compare average co-contraction during the phases, with the within–subject variables being the three footwear conditions (LPR, MPR, NR), two speeds (0.8 m/s, 1.6 m/s), and co-contraction indices (EMG-Track and EMG-Based). This analysis was performed on the PL/TA, PL/MG and PL/SOL. The effect size for the comparisons was determined using generalized eta squared (η_g^2) for the ANOVA, where .01 indicates a small effect, .06 indicates a medium effect, and 0.14 indicates a large effect. Mauchly's test of sphericity was used to test whether the assumption of sphericity was met in the repeated measures ANOVA. If the assumption of sphericity was violated ($p<0.05$), the Greenhouse–Geisser correction was used, and the corrected degrees of freedom were reported. Post-hoc two-way ANOVAs, one-way ANOVAs, and Sidak post-hoc tests were conducted when significant interaction or main effects were observed to determine the specific location of the differences. When the three-way ANOVA revealed a significant interaction, follow-up two-way ANOVAs were conducted. For the Footwear by Method interaction, analyses were performed separately at each Speed (0.8 m/s and 1.6 m/s) to examine how methods influenced co-contraction across footwear conditions ($\alpha_{adj} = 0.0034$). For the Method by Speed interaction, analyses were performed separately for each Footwear condition to examine how speed influenced co-contraction across methods ($\alpha_{adj} = 0.0085$).

Data Availability

All data supporting the findings of this study are available within the paper. Data can be made available upon request dependent on review from the overseeing research ethics board.

References

1. O'Connor, S. M. & Kuo, A. D. Direction-dependent control of balance during walking and standing. *Journal of Neurophysiology* **102,** 1411–1419 (2009).
2. Bruijn, S. M. & van Dieën, J. H. Control of human gait stability through foot placement. *Journal of The Royal Society Interface* **15,** 20170816 (2018).
3. Thies, S. B., Richardson, J. K. & Ashton-Miller, J. A. Effects of surface irregularity and lighting on step variability during gait: *Gait & Posture* **22,** 26–31 (2005).
4. Dixon, P. C. *et al.* Gait adaptations of older adults on an uneven brick surface can be predicted by age-related physiological changes in strength. *Gait & Posture* **61,** 257–262 (2018).
5. Menz, H. B. Age-related differences in walking stability. *Age and Ageing* **32,** 137–142 (2003).
6. Kellis, E., Arabatzi, F. & Papadopoulos, C. Muscle co-activation around the knee in drop jumping using the co-contraction index. *Journal of Electromyography and Kinesiology* **13,** 229–238 (2003).
7. Apps, C., Sterzing, T., O'Brien, T. & Lake, M. Lower limb joint stiffness and muscle co-contraction adaptations to instability footwear during locomotion. *Journal of Electromyography and Kinesiology* **31,** 55–62 (2016).
8. Chambers, A. J. & Cham, R. Slip-related muscle activation patterns in the stance leg during walking. *Gait & Posture* **25,** 565–572 (2007).
9. Iwamoto, Y., Takahashi, M. & Shinkoda, K. Differences of muscle co-contraction of the ankle joint between young and elderly adults during dynamic postural control at different speeds. *Journal of Physiological Anthropology* **36,** (2017).

10. DaSilva., M. *et al.* Muscle co-contractions are greater in older adults during walking at self-selected speeds over uneven compared to even surfaces. *Journal of Biomechanics* **128,** 110718 (2021).
11. Krähenbühl, N., Horn-Lang, T., Hintermann, B. & Knupp, M. The subtalar joint. *EFORT Open Reviews* **2,** 309–316 (2017).
12. Unnithan, V. B., Dowling, J. J., Frost, G. & Bar-or, O. Role of cocontraction in the O2 cost of walking in children with cerebral palsy. *Medicine & Science in Sports & Exercise* **28,** 1498–1504 (1996).
13. Damiano, D. L., Martellotta, T. L., Sullivan, D. J., Granata, K. P. & Abel, M. F. Muscle Force production and functional performance in spastic cerebral palsy: Relationship of cocontraction. *Archives of Physical Medicine and Rehabilitation* **81,** 895–900 (2000).
14. Fung, J. & Barbeau, H. A dynamic EMG profile index to quantify muscular activation disorder in spastic paretic gait. *Electroencephalography and Clinical Neurophysiology* **73,** 233–244 (1989).
15. Souissi, H., Zory, R., Bredin, J. & Gerus, P. Comparison of methodologies to assess muscle co-contraction during gait. *7* **57,** 141–145 (2017).
16. Maganaris, C. N. Force–length characteristics of *in vivo* human skeletal muscle. *Acta Physiologica Scandinavica* **172,** 279–285 (2001).
17. Gordon, A. M., Huxley, A. F. & Julian, F. J. The variation in isometric tension with sarcomere length in vertebrate muscle fibres. *The Journal of Physiology* **184,** 170–192 (1966).
18. The heat of shortening and the dynamic constants of Muscle. *Proceedings of the Royal Society of London. Series B - Biological Sciences* **126,** 136–195 (1938).

19. Ingram, D., Engelhardt, C., Farron, A., Terrier, A. & Müllhaupt, P. Muscle moment-arms: A key element in muscle-force estimation. *Computer Methods in Biomechanics and Biomedical Engineering* **18,** 506–513 (2013).

20. Maharaj, J. N., Cresswell, A. G. & Lichtwark, G. A. The mechanical function of the tibialis posterior muscle and its tendon during locomotion. *Journal of Biomechanics* **49,** 3238–3243 (2016).

21. Li, G., Shourijeh, M. S., Ao, D., Patten, C. & Fregly, B. J. How well do commonly used co-contraction indices approximate lower limb joint stiffness trends during gait for individuals post-stroke? *Frontiers in Bioengineering and Biotechnology* **8,** (2021).

22. Akl, A.R. *et al.* Muscle co-activation around the knee during different walking speeds in healthy females. *Sensors* **21,** 677 (2021).

23. Assila, N., Pizzolato, C., Martinez, R., Lloyd, D. G. & Begon, M. EMG-assisted algorithm to account for shoulder muscles co-contraction in overhead manual handling. *Applied Sciences* **10,** 3522 (2020).

24. Taniguchi, T. *et al.* Relationship between fear-avoidance beliefs and muscle co-contraction in people with knee osteoarthritis. *Sensors* **24,** 5137 (2024).

25. Diamond, L. E. *et al.* Individuals with mild-to-moderate hip osteoarthritis walk with lower hip joint contact forces despite higher levels of muscle co-contraction compared to healthy individuals. *Osteoarthritis and Cartilage* **28,** 924–931 (2020).

26. Crowninshield, R. D. & Brand, R. A. A physiologically based criterion of muscle force prediction in Locomotion. *Journal of Biomechanics* **14,** 793–801 (1981).

27. Cholewicki, J. & McGill, S. M. EMG assisted optimization: A hybrid approach for estimating muscle forces in an indeterminate biomechanical model. *Journal of Biomechanics* **27,** 1287–1289 (1994).

28. Collins, J. J. The redundant nature of locomotor optimization laws. *Journal of Biomechanics* **28,** 251–267 (1995).

29. Hoang, H. X., Diamond, L. E., Lloyd, D. G. & Pizzolato, C. A calibrated EMG-informed neuromusculoskeletal model can appropriately account for muscle co-contraction in the estimation of hip joint contact forces in people with hip osteoarthritis. *Journal of Biomechanics* **83,** 134–142 (2019).

30. Banks, J. J., Umberger, B. R. & Caldwell, G. E. EMG optimization in OpenSim: A model for estimating lower back kinetics in Gait. *Medical Engineering & Physics* **103,** 103790 (2022).

31. Molinaro, D. D., King, A. S. & Young, A. J. Biomechanical analysis of common solid waste collection throwing techniques using OpenSim and an EMG-assisted solver. *Journal of Biomechanics* **104,** 109704 (2020).

32. Assila, N., Pizzolato, C., Martinez, R., Lloyd, D. G. & Begon, M. EMG-assisted algorithm to account for shoulder muscles co-contraction in overhead manual handling. *Applied Sciences* **10,** 3522 (2020).

33. MacIntosh, A. R. & Keir, P. J. An open-source model and solution method to predict co-contraction in the finger. *Computer Methods in Biomechanics and Biomedical Engineering* **20,** 1373–1381 (2017).

34. Sarshari, E. *et al.* Muscle co-contraction in an upper limb musculoskeletal model: EMG-assisted vs. standard load-sharing. *Computer Methods in Biomechanics and Biomedical Engineering* **24,** 137–150 (2020).

35. Amarantini, D., Rao, G. & Berton, E. A two-step EMG-and-optimization process to estimate muscle force during dynamic movement. *Journal of Biomechanics* **43,** 1827–1830 (2010).

36. Choi, H. Quantitative assessment of co-contraction in cervical musculature. *Medical Engineering & Physics* **25,** 133–140 (2003).

37. Granata, K. P., Lee, P. E. & Franklin, T. C. Co-contraction recruitment and spinal load during isometric trunk flexion and extension. *Clinical Biomechanics* **20,** 1029–1037 (2005).

38. De Groote, F., Kinney, A. L., Rao, A. V. & Fregly, B. J. Evaluation of direct collocation optimal control problem formulations for solving the muscle redundancy problem. *Annals of Biomedical Engineering* **44,** 2922–2936 (2016).

39. Anderson, F. C. & Pandy, M. G. Dynamic optimization of human walking. *Journal of Biomechanical Engineering* **123,** 381–390 (2001).

40. Sousa, A. S. P. Antagonist co-activation during short and medium latency responses in subjects with chronic ankle instability. *Journal of Electromyography and Kinesiology* **43**, 168–173 (2018).

41. Tretriluxana, J., Nanbancha, A., Sinsurin, K., Limroongreungrat, W. & Wang, H.-K. Neuromuscular control of the ankle during pre-landing in athletes with chronic ankle instability: Insights from statistical parametric mapping and muscle co-contraction analysis. *Physical Therapy in Sport* **47,** 46–52 (2021).

42. Saki, F., Tahayori, B. & Bakhtiari Khou, S. Female athletes with ligament dominance exhibiting altered hip and ankle muscle co-contraction patterns compared to healthy individuals during single-leg landing. *Gait & Posture* **93,** 225–229 (2022).

43. Hellmann, D. *et al.* Influence of oral motor tasks on postural muscle activity during dynamic reactive balance. *J of Oral Rehabilitation* **51**, 1041–1049 (2024).

44. Jie, L. J. *et al.* The effects of conscious movement processing on the neuromuscular control of posture. *Neuroscience,* **509**, 63-73 (2022).

45. Klein, P., Mattys, S. & Rooze, M. Moment arm length variations of selected muscles acting on talocrural and subtalar joints during movement: An in vitro study. *Journal of Biomechanics* **29,** 21–30 (1996).

46. Peterson, D. S. & Martin, P. E. Effects of age and walking speed on coactivation and cost of walking in healthy adults. *Gait & Posture* **31,** 355–359 (2010).

47. Piche, E. *et al.* Metabolic cost and co-contraction during walking at different speeds in young and old adults. *Gait & Posture* **91,** 111–116 (2022).

48. Delabastita, T. *et al.* Distal-to-proximal joint mechanics redistribution is a main contributor to reduced walking economy in older adults. *Scandinavian Journal of Medicine & Science in Sports* **31,** 1036–1047 (2021).

49. Disselhorst-Klug, C., Schmitz-Rode, T. & Rau, G. Surface electromyography and muscle force: Limits in sEMG–force relationship and new approaches for applications. *Clinical Biomechanics* **24**, 225–235 (2009).

50. Maharaj, J. N., Cresswell, A. G. & Lichtwark, G. A. Tibialis anterior tendinous tissue plays a key role in energy absorption during human walking. *Journal of Experimental Biology* **222**, jeb191247 (2019).

51. John, C. T., Anderson, F. C., Higginson, J. S. & Delp, S. L. Stabilisation of walking by intrinsic muscle properties revealed in a three-dimensional muscle-driven simulation. *Computer Methods in Biomechanics and Biomedical Engineering* **16,** 451–462 (2013).

52. Buchanan, T. S., Lloyd, D. G., Manal, K. & Besier, T. F. Neuromusculoskeletal Modeling: Estimation of Muscle Forces and joint moments and movements from measurements of Neural Command. *Journal of Applied Biomechanics* **20,** 367–395 (2004).

53. Akl, A.R., Conceição, F. & Richards, J. An exploration of muscle co-activation during different walking speeds and the association with lower limb joint stiffness. *Journal of Biomechanics* **157,** 111715 (2023).

54. de David, A. C., Carpes, F. P. & Stefanyshyn, D. Effects of changing speed on knee and ankle joint load during walking and running. *Journal of Sports Sciences* **33,** 391–397 (2014).

55. Eerdekens, M., Deschamps, K. & Staes, F. The impact of walking speed on the kinetic behaviour of different foot joints. *Gait & Posture* **68,** 375–381 (2019).

56. Wang, R. & Gutierrez-Farewik, E. M. The effect of subtalar inversion/eversion on the dynamic function of the tibialis anterior, soleus, and gastrocnemius during the stance phase of gait. *Gait & Posture* **34,** 29–35 (2011).

57. Lenhart, R. L., Francis, C. A., Lenz, A. L. & Thelen, D. G. Empirical evaluation of gastrocnemius and soleus function during walking. *Journal of Biomechanics* **47,** 2969–2974 (2014).

58. Knarr, B. A., Zeni, J. A. & Higginson, J. S. Comparison of electromyography and joint moment as indicators of co-contraction. *Journal of Electromyography and Kinesiology* **22,** 607–611 (2012).

59. Dembia, C. L., Bianco, N. A., Falisse, A., Hicks, J. L. & Delp, S. L. OpenSim Moco: Musculoskeletal Optimal Control. *PLOS Computational Biology* **16,** (2020).

60. Zajac, F. E. Muscle and tendon: properties, models, scaling, and application to biomechanics and motor control. *Crit Rev Biomed Eng* **17**, 359-411 (1989).

61. Asmussen, M. J., von Tscharner, V. & Nigg, B. M. Motor unit action potential clustering—theoretical consideration for muscle activation during a motor task. *Frontiers in Human Neuroscience* **12**, (2018).

62. Krishnamoorthy, V., Goodman, S., Zatsiorsky, V. & Latash, M. L. Muscle synergies during shifts of the center of pressure by standing persons: Identification of muscle modes. *Biological Cybernetics* **89,** 152–161 (2003).

63. Holcomb, A. E. et al. Musculoskeletal adaptation of young and older adults in response to challenging surface conditions. *Journal of Biomechanics* **144**, 111270 (2022).

64. Willems, T. et al. Proprioception and Muscle Strength in Subjects With a History of Ankle Sprain and Chronic Instability. *J Athl Train* **37**, (2002).

65. Louwerens, J. W., Linge, B. van, de Klerk, L. W., Mulder, P. G. & Snijders, C. J. Peroneus longus and tibialis anterior muscle activity in the stance phase: A quantified electromyographic study of 10 controls and 25 patients with chronic ankle instability. *Acta Orthopaedica Scandinavica* **66**, 517–523 (1995).

66. Mark Coglianese, T. H. Alterations in Evertor/Invertor muscle activation and cop trajectory during a forward lunge in participants with functional ankle instability. *Clinical Research on Foot & Ankle* **22**, (2014).

67. Li, Y. *et al.* Does chronic ankle instability influence lower extremity muscle activation of females during landing? *Journal of Electromyography and Kinesiology* **38,** 81–87 (2018).

68. Thoma, L. M. *et al.* Muscle co-contraction during gait in individuals with articular cartilage defects in the knee. *Gait & Posture* **48,** 68–73 (2016).

69. Falconer, K., & Winter, D. A. Quantitative assessment of co-contraction at the ankle joint in walking. *Electroencephalography and Clinical Neurophysiology* **25**, 135-149 (1985).

70. Rudolph, K. S., Axe, M. J. & Snyder-Mackler, L. Dynamic stability after ACL injury: Who can hop? *Knee Surgery, Sports Traumatology, Arthroscopy* **8,** 262–269 (2000).

71. Fukunaga, T., Roy, R. R., Shellock, F. G., Hodgson, J. A. & Edgerton, V. R. Specific tension of human plantar flexors and dorsiflexors. *Journal of Applied Physiology* **80,** 158–165 (1996).

72. Naik, G. Computational Intelligence in Electromyography Analysis - A Perspective on Current Applications and Future Challenges. 177-187. (InTech, 2012).

73. Quinzi, F., Camomilla, V., Felici, F., Di Mario, A. & Sbriccoli, P. Agonist and antagonist muscle activation in elite athletes: Influence of age. *European Journal of Applied Physiology* **115,** 47–56 (2014).

74. Leardini, A. *et al.* Rear-foot, mid-foot and fore-foot motion during the stance phase of gait. *Gait & Posture* **25,** 453–462 (2007).

75. Menant, J. C., Steele, J. R., Menz, H. B., Munro, B. J. & Lord, S. R. Effects of walking surfaces and footwear on temporo-spatial gait parameters in young and older people. *Gait & Posture* **29,** 392–397 (2009).
76. Rajagopal, A. *et al.* Full-body musculoskeletal model for muscle-driven simulation of human gait. *IEEE Transactions on Biomedical Engineering* **63,** 2068–2079 (2016).
77. Ward, S. R., Eng, C. M., Smallwood, L. H. & Lieber, R. L. Are current measurements of lower extremity muscle architecture accurate? *Clinical Orthopaedics and Related Research* **467,** 1074–1082 (2008).
78. Handsfield, G. G., Meyer, C. H., Hart, J. M., Abel, M. F. & Blemker, S. S. Relationships of 35 lower limb muscles to height and body mass quantified using MRI. *Journal of Biomechanics* **47,** 631–638 (2014).
79. Maharaj, J. N. *et al.* Modelling the complexity of the foot and ankle during human locomotion: The development and validation of a multi-segment foot model using biplanar videoradiography. *Computer Methods in Biomechanics and Biomedical Engineering* **25,** 554–565 (2021).
80. Delp, S. L. *et al.* OpenSim: Open-source software to create and analyze dynamic simulations of movement. *IEEE Transactions on Biomedical Engineering* **54,** 1940–1950 (2007).
81. Nguyen, V. Q., Johnson, R. T., Sup, F. C. & Umberger, B. R. Bilevel optimization for cost function determination in dynamic simulation of human gait. *IEEE Transactions on Neural Systems and Rehabilitation Engineering* **27,** 1426–1435 (2019).

82. Banks, J. J., Umberger, B. R. & Caldwell, G. E. EMG optimization in OpenSim: A model for estimating lower back kinetics in Gait. *Medical Engineering & Physics* **103,** 103790 (2022).

83. Weng, J., Hashemi, E. & Arami, A. Human gait cost function varies with walking speed: An Inverse Optimal Control Study. *IEEE Robotics and Automation Letters* **8,** 4777–4784 (2023).

84. Hallal, C. Z., Marques, N. R., Spinoso, D. H., Vieira, E. R. & Gonçalves, M. Electromyographic patterns of lower limb muscles during apprehensive gait in younger and older female adults. *Journal of Electromyography and Kinesiology* **23,** 1145–1149 (2013).

85. Andersson, J. A. E., Gillis, J., Horn, G., Rawlings, J. B. & Diehl, M. CasADi: a software framework for nonlinear optimization and optimal control. *Math. Prog. Comp.* **11**, 1–36 (2019).

86. Wächter, A. & Biegler, L. T. On the implementation of an interior-point filter line-search algorithm for large-scale nonlinear programming. *Math. Program.* **106**, 25–57 (2006).

87. Hof, A. L. & Duysens, J. Responses of human ankle muscles to mediolateral balance perturbations during walking. *Human Movement Science* **57,** 69–82 (2018).

88. van Leeuwen, A. M., van Dieën, J. H., Daffertshofer, A. & Bruijn, S. M. Ankle muscles drive mediolateral center of pressure control to ensure stable steady state gait. *Scientific Reports* **11**, 21481 (2021).

89. Simon, S. R., Mann, R. A., Hagy, J. L. & Larsen, L. J. Role of the posterior calf muscles in normal gait. *The Journal of Bone & Joint Surgery* **60,** 465–472 (1978).

90. Sherman, M. A., Seth, A. & Delp, S. L. What is a moment arm? calculating muscle effectiveness in biomechanical models using generalized coordinates. *International Conference on Multibody Systems, Nonlinear Dynamics, and Control 7**B**,* (2013).

91. Asmussen, M. J., Lichtwark, G. A. & Maharaj, J. N. The subtalar joint maintains "spring-like" function while running in footwear that perturbs foot pronation. *J. Appl. Biomech.* **38**, 221–231 (2022).

ACKNOWLEDGEMENTS

This work was funded by the Natural Sciences and Engineering Research Council of Canada and the Canada Research Chair Program to MJA.

AUTHOR INFORMATION

Authors and Affiliations
Department of Biomedical Engineering, University of Calgary, Calgary T2N 1N4, Canada
Banin M. Al-Shimari, Vivian T. Nguyen, W. Brent Edwards, Ranita H. K. Manocha

Department of Biology, Mount Royal University, Calgary T3E 6K6, Canada
Marco J. Perizzolo

McCaig Institute for Bone and Joint Health, University of Calgary, Calgary T2N 4Z6, Canada
Sarah L. Manske, W. Brent Edwards, Ranita H. K. Manocha

Department of Radiology, Cumming School of Medicine, University of Calgary, Calgary T2N 2T9, Canada
Sarah L. Manske

Division of Physical Medicine and Rehabilitation, Cumming School of Medicine, University of Calgary, Calgary T2N 1N4, Canada
Ranita H. K. Manocha

Human Performance Laboratory, Faculty of Kinesiology, University of Calgary, Calgary T2N 1N4, Canada
W. Brent Edwards, Michael J. Asmussen

Department of Kinesiology, Vancouver Island University, Nanaimo V9R 5S5, British Columbia
Michael J. Asmussen

Contributions Statement
Conceptualization: B.M.A, M.J.A
Data Curation: B.M.A
Formal Analysis: B.M.A
Funding Acquisition: M.J.A
Investigation: B.M.A, V.T.N, M.J.P, M.J.A
Methodology: B.M.A
Software: B.M.A, M.J.A
Experiment: B.M.A
Supervision: M.J.A
Validation: B.M.A, M.J.A
Visualization: B.M.A
Writing – original draft: B.M.A with contributions from M.J.A
Writing – reviewing and editing: B.M.A, V.T.N, M.J.P, S.L.M, R.H.K.M, W.B.E, M.J.A
All authors have read and agreed to the published version of the manuscript

Corresponding author
Correspondence to Banin M. Al-Shimari

ETHICS DECLARATION

Conflicts of Interest

The authors have no conflicts of interest to disclose.